Available online at www.sciencedirect.com
ScienceDirect
ELSEVIER
Desalination 202 (2007) 333–342
DESALINATION
www.elsevier.com/locate/desal

Interactions controlling biopolymer fouling of reverse osmosis membranes

Suhan Kim[a]*, Eric M.V. Hoek[b]

[a]*Department of Environmental Science and Engineering, Gwangju Institute of Science and Technology (GIST), Gwangju, 500-712, South Korea*
Tel. +82 62 970-3282; Fax +82 62 970-2434; email: suhankim@gist.ac.kr
[b]*Department of Civil and Environmental Engineering, University of California, Los Angeles, CA, 90095, USA*

Received 31 July 2005; accepted 23 December 2005

Abstract

Laboratory experiments and model calculations were performed to elucidate the fundamental interactions that control organic fouling in reverse osmosis (RO) processes. Bovine serum albumin and alginic acid were selected as model aquatic organic macromolecules (organic foulants). An extended Derjaguin-Landau-Verwey-Overbeek (DLVO) characterization analysis was used to elucidate mechanisms of organic matter fouling on a commercial, polyamide composite RO membrane. Surface tension parameters derived from contact angle analyses are used to demonstrate that the apparent thermodynamic stability of macromolecules determines and adhesive free energy between membranes and macromolecules explained the observed differences in flux decline. Further, foulant–membrane and foulant–foulant interfacial forces helped explain why hydrophilic macromolecules formed polarization layers causing minimal flux decline, while hydrophobic macromolecules formed gel (or cake) layers that led to severe flux decline.

Keywords: Reverse osmosis; Organic fouling; Extended DLVO; Modeling

1. Introduction

Fouling by organic matter is one of the key performance limitations of reverse osmosis (RO) processes used to treat both traditional and non-traditional water sources. Natural organic macromolecules (geopolymers and biopolymers) often pass through conventional and membrane filtration pre-treatment processes, and thus, are among the most problematic foulants for downstream RO treatment systems. Among non-traditional, or alternative, water sources municipal wastewater is perhaps the most important because it is the only alternative water source with a guaranteed supply that expands with an increasing population and economy.

*Corresponding author.

Presented at the conference on Wastewater Reclamation and Reuse for Sustainability (WWRS2005), November 8–11, 2005, Jeju, Korea. Organized by the International Water Association (IWA) and the Gwangju Institute of Science and Technology (GIST).

0011-9164/06/$– See front matter
doi:10.1016/j.desal.2005.12.072

Hence, our focus in this study is on biopolymer fouling of RO membranes. Our hypothesis was that deposition of organic macromolecules can be reasonably described following the classical approaches for characterizing colloidal deposition in membrane processes.

The classical Derjaguin-Landau-Verwey-Overbeek (DLVO) theory has been frequently used to describe colloidal deposition, but quite often DLVO fails to accurately describe experimental observations. The addition of Lewis acid–base interactions to classical DLVO theory corrects many of these inconsistencies. This approach is often called the "extended DLVO" or "XDLVO" theory [1]. However, a more complete description of the forces governing colloidal deposition in membrane processes includes interfacial hydrodynamic interactions, especially the drag force imparted by water permeation [2,3].

In this study, the theoretical approach used to understand organic fouling of RO membranes employs the interfacial force balance approach of Wang et al. [3], which combines interfacial hydrodynamic and XDLVO interactions to describe colloidal deposition. Model organic macromolecules were characterized, RO fouling studies were conducted, and fouling behavior was analyzed. Using the interfacial force balance approach of Wang et al. [3], we determine the magnitude of forces as a function of separation distance to gain insight about which interfacial forces govern biopolymer fouling of RO membranes.

2. Materials and methods

2.1. Membrane, reagents, and foulants

The RO membrane used in this study was designated by the manufacturer as XLE (DowFilmTec Corp., Edina, MN, USA). Salt stock solutions were prepared using ACS grade NaCl dissolved in deionized water (DI). Bovine serum albumin (BSA) and alginic acid (AA) (alginic acid sodium salt from brown algae, Sigma-Aldrich Corp., St. Louis, MO, USA) were used as model organic foulants. BSA is purified by heat treatment and organic solvent precipitation and makes up approximately 50% of the total protein in bovine blood serum. AA is a straight chain, hydrophilic, polyuronic acid composed primarily of anhydro-β-D-mannuronic acid residues with $1 \rightarrow 4$ linkage.

Electrophoretic mobility and hydrodynamic radii of foulants were determined by particle electrophoresis and dynamic light scattering (ZetaPALS, Brookhaven Instruments Corp., Holtsville, NY, USA). The electrophoretic mobility data were used to calculate zeta potential using Smolchowski equation. The zeta potential of membrane was determined from streaming potential measurements (EKA, Anton Parr, Austria). Surface tensions of foulants and membrane were determined from measured contact angles (VCA-1000, AST Products Inc., Billerica, MA, USA) of DI, ethylene glycol (EG), and diiodomethane (DM) by the sessile drop method on foulant layers filtered by a membrane or on a clean membrane.

2.2. Fouling experiment procedure

2.2.1. Crossflow membrane filter

The crossflow membrane filter (CMF) used in fouling experiments was a modified version of a commercially available stainless steel CMF unit (Sepa CF, Osmonics, Inc.; Minnetonka, MN, USA). A schematic illustration of the experimental apparatus and a complete description of modifications are provided elsewhere [4]. The CMF was rated for operating pressures up to 6895 kPa (1000 psi) and had channel dimensions of 14.6 cm, 9.5 cm, and 1.73 mm for channel length, width, and height, respectively. Membrane surface area was $1.39 \times 10^{-2} m^2$ and cross-sectional flow area was $1.64 \times 10^{-4} m^2$.

2.2.2. Membrane resistance

At the start of each fouling experiment, deionized water was filtered through the membrane for 16–24 h to allow for membrane compaction and other unknown causes of flux decline inherent to laboratory-scale recirculation systems. After stable flux was achieved, the membrane hydraulic resistance was determined by measuring pure water flux over a range of applied pressures. The relationship governing the experimental pure water flux is

$$v_w = \frac{\Delta P}{\mu R_m} \quad (1)$$

where R_m indicates the membrane hydraulic resistance (the inverse of membrane permeability), v_w the pure water flux, ΔP the applied pressure, and μ the dynamic viscosity of water. Membrane resıstance was determined from a linear regression of the measured pure water flux and applied pressure data.

2.2.3. Osmotic pressure and salt rejection

After membrane hydraulic resistance was determined, an electrolyte solution was added to provide the desired feed ionic composition. Flux and crossflow were set at the desired values for each fouling experiment and the system was allowed to equilibrate for up to 24 h to ensure stable performance. Due to concentration polarization of rejected ionic constituents, the driving force for permeation is the difference between the applied pressure and the transmembrane osmotic pressure ($\Delta\pi_m$). Thus, the permeate flux prior to addition of organic foulants is described by

$$v_0 = \frac{\Delta P - \Delta\pi_m}{\mu R_m} \quad (2)$$

The effective transmembrane osmotic pressure was determined for steady state conditions using Eq. (2) since flux, applied pressure, water viscosity, and membrane hydraulic resistance were known. During electrolyte equilibration, observed salt rejection (R_o) was determined from feed and permeate conductivity measurements. Conductivity of NaCl solutions was determined to be linear over the range of ionic strengths used and for all salts tested.

2.2.4. Accelerated fouling experiments

Accelerated fouling experiments were conducted at the same initial water flux. After the pure water and electrolyte equilibrations described above, a dose of foulant was added to the feed tank to provide the appropriate particle feed concentration. This was time equal to zero for all fouling experiments. Flux was monitored continuously for the duration of the experiment and recorded in real-time on a laboratory computer. Conductivity, pH, and turbidity measurements were made at the start, end, and at several points during the fouling experiment to monitor feed and permeate solution properties. The fouling experiments were performed with full recirculation (permeate and retentate recycled to the feed tank). Temperature was maintained at 25°C by a recirculating chiller. The operation was conducted at initial flux of 7.54×10^{-6} m/s, crossflow Reynolds number of 293, and unadjusted pH of 5.8 ± 0.2. Concentrations of salt and foulants were 50 mM and 60 mg/L, respectively.

2.3. Interfacial free energy analysis

Surface thermodynamic parameters were determined from measured sessile drop contact angles on membranes and membrane filtered organic deposit layers using the three liquid extended DLVO approach of van Oss [5]. The total surface tension (γ^{TOT}) of any media is the sum of Lifshitz-van der Waals (apolar) and acid–base (polar) components. Thus,

$$\gamma^{TOT} = \gamma^{LW} + \gamma^{AB}, \quad (3)$$

where γ^{LW} is the Lifshitz-van der Waals component, γ^{AB} ($=2\sqrt{\gamma^+\gamma^-}$) is the acid–base component, γ^+ and γ^- and are the electron-acceptor and electron-donor components, respectively. Individual surface tension components γ^{LW}, γ^+, and γ^- are determined from contact angles measured using three probe liquids of known surface tension calculated by the extended Young equation

$$\left(1+\frac{\cos\theta}{r}\right)\gamma_l^{TOT}=2\left(\sqrt{\gamma_s^{LW}\gamma_l^{LW}}+\sqrt{\gamma_s^+\gamma_l^-}+\sqrt{\gamma_s^-\gamma_l^+}\right) \quad (4)$$

where θ is the equilibrium contact angle of the liquid on the surface, r accounts for the increase in surface area due to roughness (a.k.a., "Wenzel's roughness ratio" as determined by AFM for the membrane) and the subscripts s and l represent the solid surface and the probe liquid, respectively.

The interfacial free energy per unit area between surfaces 1 and 2 immersed in liquid 3 gives an indication of the stability of a material immersed in a liquid medium. If the free energy is positive, a material is thought to be stable (lyophilic generally, or hydrophilic if the liquid is water), and if negative it is unstable (lyophobic/hydrophobic). The interfacial free energy is determined from

$$\Delta G_{h_0}^{LW}=2\left(\sqrt{\gamma_3^{LW}}-\sqrt{\gamma_1^{LW}}\right)\left(\sqrt{\gamma_2^{LW}}-\sqrt{\gamma_3^{LW}}\right) \quad (5a)$$

$$\begin{aligned}\Delta G_{h_0}^{AB}=&\,2\sqrt{\gamma_3^+}\left(\sqrt{\gamma_1^-}+\sqrt{\gamma_2^-}-\sqrt{\gamma_3^-}\right)\\&+2\sqrt{\gamma_3^-}\left(\sqrt{\gamma_1^+}+\sqrt{\gamma_2^+}-\sqrt{\gamma_3^+}\right)\\&-2\sqrt{\gamma_1^+\gamma_2^-}-2\sqrt{\gamma_1^-\gamma_2^+}\end{aligned} \quad (5b)$$

where $\Delta G_{h_0}^{LW}$ and $\Delta G_{h_0}^{AB}$ are Liftshitz-van der Waals and acid–base interaction free energy components at the separation distance of h_0, respectively, while the subscript h_0 represents the minimum separation distance of 0.157 ± 0.009 nm [5]. If surfaces 1 and 2 are different materials (e.g., a foulant and membrane), then the sum is the interfacial free energy of adhesion between the dissimilar materials. If surfaces 1 and 2 are composed of identical materials (e.g., two identical foulants), then the sum of $\Delta G_{h_0}^{AB}$ and $\Delta G_{h_0}^{LW}$ is the interfacial free energy of cohesion for that material.

DM is an apolar liquid, and according to theory, the contact angle of an apolar liquid of known surface tension can be used to determine the van der Waals component of the solid surface tension. The combination of measured contact angles and known surface tensions of the polar liquids (water and EG) can then be used to determine the electron donor and electron acceptor components of the solid surface tension. The van der Waals, electron donor, and electron acceptor surface tensions are then used to derive free energy of cohesion between like materials and the free energy of adhesion between different materials.

2.4. Interfacial force analysis

When a foulant is introduced into the membrane channel, the hydrodynamic forces and interfacial forces determine the transport and deposition of a foulant. The interfacial forces, including Liftshitz-van der Waals (F_{LW}) electrostatic (F_{EL}), and acid–base (F_{AB}) interaction forces, are calculated using spherical hydrodynamic radii determined by light scattering for each of the foulants. The expressions for these forces are

$$F_{LW}=2\pi h_0^2\Delta G_{clm}^{LW}a_p\left(\frac{1}{h^2}\right)\left(1+\frac{5.32h}{\lambda_{LW}}\right)^{-1} \quad (6a)$$

$$F_{EL}=64\pi\kappa\varepsilon_0\varepsilon_r a_p\left(\frac{kT}{ze}\right)^2\gamma_c\gamma_s\exp\left(-\frac{h}{\lambda_{EL}}\right) \quad (6b)$$

$$F_{AB}=2\pi a_p\Delta G_{clm}^{AB}\exp\left(\frac{h_0-h}{\lambda_{AB}}\right) \quad (6c)$$

where, ΔG_{clm}^{LW} and ΔG_{clm}^{AB} are the LW interaction and the acid–base interaction energy components between the colloidal foulant (c) and a membrane (m) in the liquid (l), which are obtained from the surface energy analysis described above. In Eq. (6a), a_p is the radius of the colloidal particle, λ_{LW} (≅100 nm) is the characteristic decay length of LW interaction in water, h is the separation distance between the colloid and the surface. In Eq. (6b), λ_{EL}^{-1} ($=3.28\times10^{9}\sqrt{c_{NaCl}}$, c_{NaCl} in moles per liter) is the reciprocal of the Debye length, ε_0 ($=8.85\times10^{-12}$ C^2/ J/ m) the absolute permitivity of free surface, ε_r (=78.9) is the dielectric constant of water, z is the valance of the ion, e is the electron charge ($=1.6\times10^{-19}$ C), $\gamma_{c/s}$ and $\zeta_{c/s}$ are the dimensionless zeta potential ($=\tanh[ze\zeta_{c/s}/4kT$) and the actual zeta potential of the colloid and the surface, respectively, k is Boltzman constant ($=1.38\times10^{-23}$ J/K), T is the absolute temperature. In Eq. (6c), λ_{AB} (≅0.6 nm) is the characteristic decay length of AB interactions in water. All the interfacial forces decay with the increase of separation distance between a colloid and surface.

The actual permeation drag force (F_{PD}) experienced by a particle approaching a membrane surface can be expressed as [6]

$$F_{PD} = -\left(6\pi\mu v_w a_p\right)\cdot\varphi_H, \tag{7}$$

which is the product of Stoke's drag and an interfacial hydrodynamic correction factor (φ_H). The interfacial hydrodynamic correction factor accounts for an increasing force resisting the approach of a spherical particle to a flat permeable (i.e., membrane) surface. It is a function of particle size, the Darcy resistance of the permeable surface, particle–surface separation distance and must be computed numerically [2]. Goren's correction factor increases sharply as a particle approaches a membrane surface. The maximum value occurs at the contact and is described analytically by

$$\varphi_{H,h_0} = \left[\frac{2R_t a_p}{3} + (1.072)^2\right]^{1/2} \tag{8}$$

where R_t is the total hydraulic resistance of a membrane filtration system ($R_t = R_m + R_c$). Permeation drag force increases with the decrease of separation between a particle and membrane. This increase in the drag force tends to decrease the transverse component of particle velocity as it approaches the wall and hence has been termed hydrodynamic retardation, which is physically due to the slow drainage of the fluid from between the two solid surfaces [7].

3. Results and discussion

3.1. Membrane and foulant characterization

Key physicochemical properties of the membrane and macromolecules are reported in Table 1. BSA and AA appear to be well described by spherical radii of 5–7 nm. It is worth noting that alginate appears to take on a globular (pseudo-spherical) conformation at the solution chemistry tested, and thus, can reasonably be treated as a spherical colloid. All materials exhibit significant negative zeta potentials at 50 mM NaCl and unadjusted pH of 5.8 ± 0.2. Based on our experience with membrane fouling, we consider a material hydrophilic if it produces a pure water contact angle less than about 45 degrees. Hence, contact angle data indicates that BSA is quite hydrophilic, while AA and XLE are moderately hydrophobic.

Table 2 provides calculated surface tension parameters (γ^{LW}, γ^{+}, γ^{-}, γ^{AB}, and γ^{TOT}) of the experimental materials along with the calculated membrane–membrane or foulant–foulant free energies of interaction (at contact). Surface tension parameters were calculated first using Eqs. (3) and (4), and the contact angle data. Then, the LW and AB components of the surface free energy at the contact were calculated using Eq. (5) and the previously determined

Table 1
Foulant and membrane physicochemical properties

Characteristics		Membrane	Foulant	
		XLE	BSA	AA
Mean DLS[a] diameter (nm)		N.A.	6.7 ± 4.0	5.4 ± 3.7
Zeta potential[b] (mV)		–14.4 ± 3.0	–15.6 ± 6.1	–17.1 ± 4.6
Contact angle (°)	w/ DI	67.6 ± 0.3	18.4 ± 3.2	52.5 ± 6.4
	w/ EG	14.8 ± 1.1	23.1 ± 0.3	8.5 ± 3.0
	w/ DM	18.2 ± 0.9	36.5 ± 0.6	33.0 ± 2.3

[a]Dynamic light scattering.
[b]Zeta potential was measured in 50 mM of NaCl solution at pH 5.8 ± 0.2.

surface tension parameters. The sum of LW and AB free energy components for a given material gives the surface free energy of cohesion [5]. In determining the cohesive free energy for a single material, surfaces 1 and 2 in Eq. (5).

A negative cohesive free energy value suggests a material is thermodynamically unstable, while a positive cohesive free energy suggests thermodynamic stability. Hence, BSA is considered stable in water, while AA and XLE are inherently unstable. However, an important consideration, especially with regard to the apparent stability of the macromolecules in water, is the kinetic stabilization that occurs through electrostatic double layer interactions imparted by the macromolecule zeta potentials. Both BSA and AA possess significant negative charge density due to carboxylate and other acidic moieties.

The surface free energy at contact between two different materials describes the strength of adhesion between two surfaces at contact. Table 3 shows the adhesive free energy parameters between the model foulants and the RO membrane. The adhesive free energy is calculated the same way as the cohesive surface free energy; however, in Eq. (5) the surfaces 1 and 2 are different materials and thus have different surface tension parameters. According to the data in Table 3, both foulants exhibit strong adhesion when in contact with the XLE membrane surface, which means that the foulants should adhere strongly to XLE once deposited onto the membrane surface. However, foulant deposition

Table 2
Surface tension parameters and interfacial free energy of cohesion

Parameters	γ^{LW}	γ^{+}	γ^{-}	γ^{AB}	γ^{TOT}	ΔG_{sls}^{LW}	ΔG_{sls}^{AB}	ΔG_{sls}^{CO}
Membrane								
XLE	37.19	0.67	7.89	4.61	41.81	–4.09	–37.90	–41.98
Foulants								
BSA	26.71	0.00	39.51	0.32	33.77	–0.50	24.84	24.34
AA	27.44	0.19	19.22	3.85	44.64	–0.65	–12.28	–12.93

Table 3
Interfacial free energy of adhesion between foulants and XLE membrane

Parameters	ΔG_{slm}^{LW}	ΔG_{slm}^{AB}	ΔG_{slm}^{AB}
BSA	–1.43	–12.1	–13.5
AA	–1.63	–26.3	–27.9

onto membranes is governed by the interplay between interfacial hydrodynamic and XDLVO interactions as described above.

3.2. Flux decline and interfacial free energy

Accelerated laboratory-scale fouling experiments were performed following the experimental procedures described above. Fig. 1 is a representative set of flux decline data for the XLE membrane using BSA and AA as model foulants. All experimental conditions were the same except the model foulant that was tested. In the first 15 min of operation, both BSA and AA caused similar rates of flux decline. However, beyond about 20–30 min there was no additional flux decline for the BSA suspension. In contrast, the AA suspension produced a continual loss of flux that did not level off over the duration of the experiment. Flux decline due to organic fouling is attributed to an additional hydraulic resistance imparted by the combination of macromolecular polarization and gel layers.

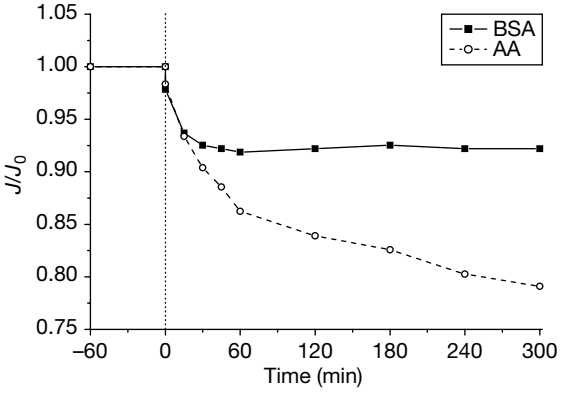

Fig. 1. Flux decline due to organic fouling.

Understanding the difference in observed flux decline is facilitated by a conceptual analysis of the foulant deposition. In general, three fundamental mechanisms contribute to particle deposition in membrane systems: convection, diffusion, and interfacial forces. First, transport of foulants to the membrane–solution interface occurs by a combination of permeate convection and Brownian diffusion. Second, initial foulant deposition is largely determined by the balance of permeate drag and foulant–membrane interfacial forces. Hence, the initial deposition of foulants is influenced by interfacial free energy of adhesion (foulant–membrane interactions). Third, after a foulant deposit layer forms, subsequent and long-term foulant deposition is governed by the balance of permeation drag and foulant–foulant interfacial forces. In other words, the formation of a foulant deposit layer on the membrane surface modifies the surface properties to be effectively those of the macromolecule. In this case, foulant deposition is influenced by interfacial free energy of cohesion (foulant–foulant interactions). It is probable that substantially more than a monolayer of macromolecules must accumulate in order to completely mask the clean membrane surface properties due to the rough morphology of polyamide membrane surfaces.

Both BSA and AA have favorable (attractive) interfacial free energies of adhesion with the XLE membrane. The free energies of adhesion reported in Table 3 are –13.5 and –27.9 mJ/m^2. In absence of any interfacial repulsion the rate of deposition should be determined by the balance of convective and diffusive transport, which (at the same operating conditions) should be similar for the two macromolecules because of their similar hydrodynamic diameters.

AA macromolecules appear to be thermodynamically unstable, and thus, aggregation or deposition is favorable (attractive) according to the free energy of cohesion (Table 2). Hence, AA deposition is favorable on both the clean and AA modified membrane surfaces. However, BSA exhibits a positive free energy of cohesion because the sum of acid–base and van der Waals interparticle interactions is repulsive. Thus, BSA deposition appears to be minimal once a significant BSA deposit layer forms. This simple interfacial free energy analysis provides insight into the mechanisms governing foulant deposition and flux decline, but it does not consider electrostatic double layer interactions which may alter the favorability of particle deposition.

3.3. Flux decline and XDLVO interfacial forces

Fig. 2 shows the results of the force analyses for two foulants and XLE membrane. XDLVO interaction forces between a foulant and fouling layer were calculated under the assumption that both the clean and fouled membrane surfaces are flat. Force calculations were carried out using surface energy parameters, zeta potential data, and mean DLS diameters provided in Tables 1 and 2 in the hydrodynamic conditions of 740–790 kPa of constant applied pressure, 7.5×10^{-6} m/s of permeate flux, and $4.9–5.6\times10^{13}$ m^{-1} of membrane resistance. As the separation distance increases, all the interaction forces become smaller until only permeation drag

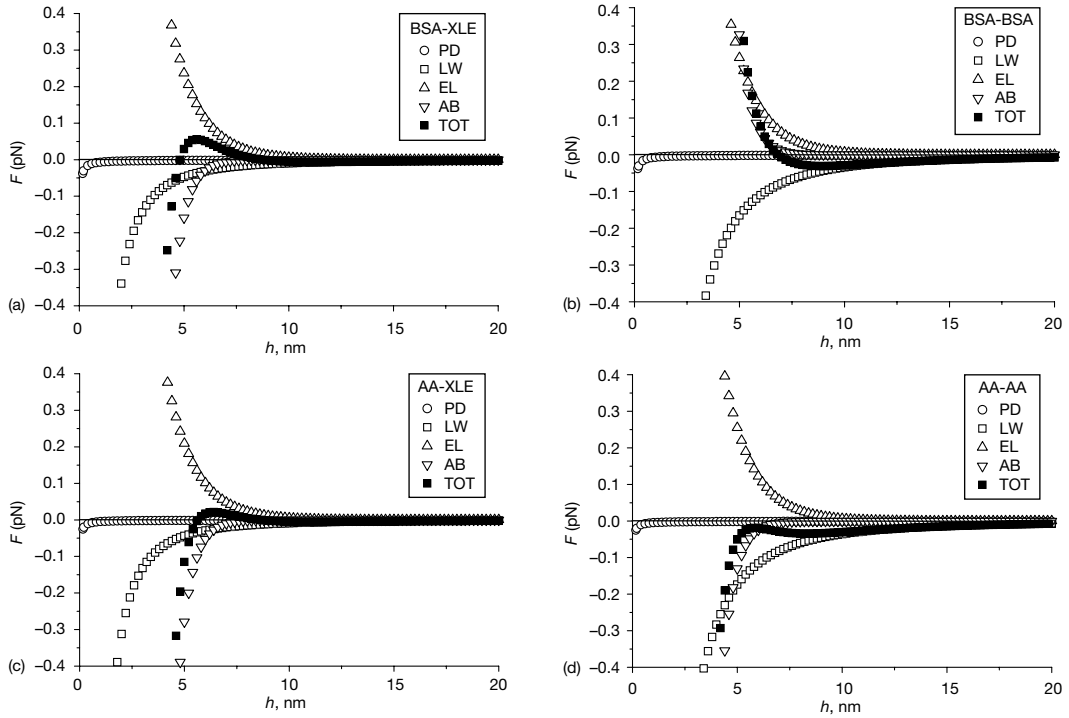

Fig. 2. Predicted interfacial forces between (a) Bovine serum albumin (BSA) particle and XLE surface, (b) BSA particle and BSA surface, (c) alginic acid (AA) particle and XLE surface, and (d) AA particle and AA surface. (PD = permeation drag force, LW = Liftshitz-van der Waals force, EL = electrostatic double layer force, AB = Lewis acid–base force, TOT = total sum of all forces).

remains at large separations. At short separations, less than about 10 nm, the total interaction force behaviors become different according to the interaction type (e.g. foulant–membrane, foulant–fouling). Within this relatively short range, the effect of permeation drag on BSA and AA was almost negligible compared to the other interfacial forces. A key factor in both cases is the dependence of Stoke's drag and Goren's hydrodynamic correction factor on the size of BSA and AA. As stated earlier, Goren's correction factor is inversely related to particle radius and very sharply decreases as particle size approaches the macromolecular range.

Attraction between foulants and XLE increase as foulants approach the membrane surface. Because the electrostatic forces start to work from rather long-range distance (~5–10 nm), strong repulsion occurs within this range of separation, but only if the electrostatic double layer repulsion is greater than attractive forces (LW and AB). This is observed for both foulants interacting with the clean XLE surface as shown in Figs. 2(a) and (c). This repulsive barrier tends to inhibit the approach of foulants to a membrane surface; however, if a foulant passes this barrier, it will deposit onto the membrane surface and be strongly adhered because of large attractive interaction force at small separations (less than ~5 nm). Initial flux decline behaviors by BSA and AA fouling are explained by this overall behavior because the presence of a repulsive barrier at small separation does not preclude deposition, it simply implies there will be a migration of macromolecules away from the membrane surface in proportion to the maximum repulsive force.

After the initial stage of operation, the fouling behavior becomes more dependent upon foulant–foulant interactions. BSA-BSA interactions becomes more repulsive as a BSA colloid approaches the fouling layer within 7 nm of separation as show in Fig. 2(b), which will prevent BSA from depositing. This explains the observed BSA fouling behavior in Fig. 1. Attractive interactions between AA macromolecules occur at separations less than 20 nm [refer to Fig. 2(d)], which means AA will easily deposit on the already formed AA fouling layer. This provides a reasonably mechanistic, albeit simple, explanation for the continuous flux decline observed for the AA suspension in Fig. 1. The simple explanation offered must be considered within the context of the very simple experimental system employed. For example, the presence of plurivalent ions (calcium, iron, etc.) may produce complexation or coagulation reactions, which destabilize the macromolecules and make the resultant fouling behavior much more complex.

4. Conclusions

Valuable insights into the mechanisms of organic matter fouling of RO membranes were gained by treating the organic macromolecules like colloidal particles. Interfacial forces between foulants and the membrane surface or between foulants and the fouled (modified) membrane surface offer reasonable explanation for the difference in flux decline behavior observed for two model organic foulants — BSA and AA from brown algae (AA). Monodisperse suspensions of thermodynamically stable macromolecules, like BSA, may result in a rapid initial flux loss followed by a constant limiting flux, whereas monodisperse suspensions of thermodynamically unstable macromolecules, like alginate, may result in rapid initial flux loss followed by a sustained flux decline. Therefore, long-term flux decline behavior is attributed to the relative repulsion or attraction of the macromolecule for itself.

In a companion paper published in this same issue, we focus on natural organic matter (NOM) fouling of ultrafiltration membranes where the organic macromolecules tested are classically considered dissolved in nature [see Lee et al., "Natural Organic Matter (NOM) Fouling due to Foulant–Membrane Physicochemical

Interactions"). The NOM used in this study has molecular weights ranging from 60 to 100 kDa and exhibits a hydrodynamic diameters of ~5–7 nm; hence, it is classically considered "colloidal," not "dissolved." Regardless, it appears that fouling by both dissolved and colloidal organic matter reasonably well described by the classical colloidal deposition approach. The experimental and theoretical results presented here provide new, fundamental insight into mechanisms of organic fouling. In future studies, fouling of RO and NF membranes will be studied using more complex suspensions comprising bacteria, biopolymers, geopolymers, and inorganic colloids.

Acknowledgements

The research described above was performed while Dr. Suhan Kim was a postdoctoral fellow at University of California, Riverside and University of California, Los Angeles. Partial financial support for this work was obtained through a post-doctoral fellowship from the Korea Science and Engineering Foundation (KOSEF) for Dr. Kim. Additional support was obtained from the California Department of Water Resources through the Desalination Research Innovation Partnership (DRIP), which is managed by the Metropolitan Water District of Southern California.

References

[1] J.A. Brant and A.E. Childress, Assessing short-range membrane-colloid interactions using surface energetics, J. Membr. Sci., 203 (2002) 257–273.

[2] S.T. Kang, A. Subramani, E.M.V. Hoek, M.A. Deshusses and M.R. Matsumoto, Direct observation of biofouling in cross-flow microfiltration: mechanisms of deposition and release, J. Membr. Sci., 244 (2004) 151–165.

[3] S. Wang, G. Guillen and E.M.V. Hoek, Direct observation of microbial adhesion to mernbranes, Environ. Sci. Technol., 39 (2005) 6461–6469.

[4] E.M.V. Hoek, A.S. Kim and M. Elimelech, Influence of crossflow membrane filter geometry and shear rate on colloidal fouling in reverse osmosis and nanofiltration separations, Environ. Eng. Sci., 19 (2002) 357–372.

[5] C.J. van Oss, Interfacial Forces in Aqueous Media, Pages, Marcel Dekker, Inc., New York, NY, 1994.

[6] S.L. Goren, Hydrodynamic force resisting the approach of a sphere to a plane permeable wall, J. Colloid Interface Sci., 69 (1979) 78–85.

[7] S. Chellam and M.R. Wiesner, Particle-transport in clean membrane filters in laminar-flow, Environ. Sci. Technol., 26 (1992) 1611–1621.